Astroparticle Physics 34 (2011) 732–737

Contents lists available at ScienceDirect

Astroparticle Physics

journal homepage: www.elsevier.com/locate/astropart

The development of a cryogenic detector with $CaMoO_4$ crystals for neutrinoless double beta decay search

S.J. Lee [a,b], J.H. Choi [a], F.A. Danevich [c], Y.S. Jang [b], W.G. Kang [d], N. Khanbekov [e], H.J. Kim [f], I.H. Kim [b], S.C. Kim [a], S.K. Kim [a,*], Y.D. Kim [d], Y.H. Kim [b,*], V.V. Kobychev [a,c], V.N. Kornoukhov [e], J.I. Lee [d], J.S. Lee [b], K.B. Lee [b], M.K. Lee [b], Y.H. Lee [b,1], S.S. Myung [a], J.H. So [f], V.I. Tretyak [c], Y. Yuryev [a]

[a] Department of Physics and Astronomy, Seoul National University, Seoul 151-747, Republic of Korea
[b] Korea Research Institute of Standards and Science, Daejon 305-340, Republic of Korea
[c] Institute for Nuclear Research, Kyiv 03680, Ukraine
[d] Physics Department, Sejong University, Seoul 143-747, Republic of Korea
[e] Institute for Theoretical and Experimental Physics, Moscow 117218, Russia
[f] Physics Department, Kyungpook National University, Daegu 702-701, Republic of Korea

ARTICLE INFO

Article history:
Received 9 July 2010
Received in revised form 7 January 2011
Accepted 15 January 2011
Available online 22 January 2011

Keywords:
Neutrinoless double beta decay
$CaMoO_4$ crystal
Cryogenic detector

ABSTRACT

The search for neutrinoless double beta decay ($0\nu\beta\beta$) is a key experiment for evaluating the mass of the neutrino and for determining the Majorana/Dirac nature of neutrinos. A scintillating $CaMoO_4$ crystal is a good material for use in investigating $0\nu\beta\beta$ with cryogenic detectors. The high transition energy ($Q = 3034$ keV) and nearly 10% natural abundance of ^{100}Mo, together with the scintillating property of the crystal, provide favorable conditions to search for $0\nu\beta\beta$ of ^{100}Mo. We report a prototype experiment operating at low temperatures using a $CaMoO_4$ crystal as a particle absorber. Prior to testing of isotopically-enriched $^{40}Ca^{100}MoO_4$ crystals, a $CaMoO_4$ crystal with Mo of natural isotopic composition was tested. Using a metallic magnetic calorimeter as a temperature sensor, we achieved high energy resolutions for alpha particles and low-energy gamma rays. This experiment shows the feasibility of scaling up the crystal size to perform a high sensitivity search for $0\nu\beta\beta$ decay of ^{100}Mo.

1. Introduction

Neutrinoless double beta decay ($0\nu\beta\beta$) [1] is a special case of double beta decay that occurs without the emission of two neutrinos. $0\nu\beta\beta$ remains hypothetical, while two neutrino double beta decay ($2\nu\beta\beta$) is observed for 10 nuclides to date [2]. The search for $0\nu\beta\beta$ has been boosted by the discovery of neutrino oscillation [3], which revealed that neutrinos are massive particles. While neutrino oscillation experiments cannot determine the individual masses of neutrinos, a measurement of the half-life of $0\nu\beta\beta$ will yield the effective mass of the neutrino. Moreover, detection of $0\nu\beta\beta$ will confirm that the neutrino is a Majorana particle [4]; that is, that the neutrino is identical to its anti-particle counterpart, the anti-neutrino.

Several experimental groups have pursued $0\nu\beta\beta$ research. A part of Heidelberg–Moscow group claimed to observe $0\nu\beta\beta$ in ^{76}Ge [5]. The NEMO 3 experiment has been used tracking detectors to investigate several different candidate materials including ^{100}Mo [6]. The GERDA experiment on ^{76}Ge [7] is under development to confirm or discard the result claimed by the Heidelberg–Moscow group. CUORICINO has measured the lower limit of half-life of $0\nu\beta\beta$ in ^{130}Te using cryogenic detectors [8].

$CaMoO_4$ crystal was proposed as a good candidate material for $0\nu\beta\beta$ search [9]. Subsequent research established the technique for growing large crystals with high light-yield suited for $0\nu\beta\beta$ search experiment [10,11]. ^{100}Mo has one of the highest transition energy (3034 keV) [12], and the level of gamma ray background radiation from the surrounding materials is expected to be low in this energy region. The fractional mass of the molybdenum element in the crystal is relatively high (about 50%). The natural abundance of ^{100}Mo is 9.82(5)% [13], and the enrichment of ^{100}Mo at the level

* Corresponding authors. Tel.: +82 2 880 6594; fax: +82 2 875 4719 (S.K. Kim), tel.: +82 42 868 5975; fax: +82 42 868 5953 (Y.H. Kim).
E-mail addresses: sjlee@hep1.snu.ac.kr (S.J. Lee), jhchoi@hep1.snu.ac.kr (J.H. Choi), danevich@kinr.kiev.ua (F.A. Danevich), crazywin@kriss.re.kr (Y.S. Jang), phiterpen@gmail.com (W.G. Kang), hongjoo@knu.ac.kr (H.J. Kim), manihe@hanmail.net (I.H. Kim), sckim@hep1.snu.ac.kr (S.C. Kim), skkim@hep1.snu.ac.kr (S.K. Kim), ydkim@sejong.ac.kr (Y.D. Kim), yhkim@kriss.re.kr (Y.H. Kim), kobychev@kinr.kiev.ua (V.V. Kobychev), kornoukhov@itep.ru (V.N. Kornoukhov), jileeeee@gmail.com (J.I. Lee), junesurlee@kriss.re.kr (J.S. Lee), lee@kriss.re.kr (K.B. Lee), mklee@kriss.re.kr (M.K. Lee), lyh1206@unitel.co.kr (Y.H. Lee), ssmyung@hep1.snu.ac.kr (S.S. Myung), jhso@knu.ac.kr (J.H. So), tretyak@kinr.kiev.u (V.I. Tretyak), yuyuryev@gmail.com (Y. Yuryev).
[1] Present address: Korea Institute of Machinery and Materials, Daejon 305-343, Republic of Korea.

0927-6505/$ - see front matter © 2011 Elsevier B.V. All rights reserved.
doi:10.1016/j.astropartphys.2011.01.004

higher than 90% can be done relatively easily by the gaseous centrifuge technique.

Because $CaMoO_4$ is a scintillating crystal, two detection channels can be used for the active rejection of an alpha background, phonon and light channels. Alpha events occuring on the crystal surface from possible radioactive contamination are one of the main sources of background that can be misinterpreted as $0\nu\beta\beta$ events [14]. Due to the different conversion ratios of incident energy into heat or scintillation between alpha and gamma/beta events; that is, different quenching factors, surface alpha events can be significantly suppressed by the additional light detection. This type of simultaneous measurement of light and phonon signals has also been reported to improve the energy resolution [15].

Moreover, $CaMoO_4$ is a highly efficient scintillator at room temperature in contrast to other molybdates, such as $PbMoO_4$ [14], Li_2MoO_4 [16], and $ZnMoO_4$ [17,18]. Therefore, one can easily test the scintillation properties of $CaMoO_4$ and measure its radiopurity at room temperature. It will simplify the detector material development process for $0\nu\beta\beta$ search experiments.

Meanwhile, double beta decaying isotope ^{48}Ca can be an important internal background source in $CaMoO_4$ due to its high transition energy of 4274 keV [11,19]. However, this background source can be eliminated by using calcium isotopically-depleted in ^{48}Ca.

Thermal detectors operating at low temperatures have shown extremely high energy resolution and a low energy threshold, and can play an important role in achieving better sensitivity in rare event experiments. A high energy resolution of the detector is critical to overcome an unavoidable background caused by the two-neutrino mode of double beta decay [20]. A metallic magnetic calorimeter (MMC) is a promising low temperature detector for a large-scale experiment [21]. MMCs use a paramagnetic material with well-understood properties as a temperature sensor under a magnetic field. The MMCs have shown state-of-the-art performance in X-ray, alpha, beta, and gamma spectroscopy [21–23]. Moreover, MMCs help to investigate the thermal properties of crystal absorbers and the detector's response to a wide range of energy inputs because of their high energy resolution, fast response time, and flexibility in the operating temperatures and magnetic fields during an experiment. By choosing the dimension of the temperature sensor and the concentration of the magnetic material in it, the detector can be scaled up to a large mass because an optimal detector minimizing the degradation of the energy sensitivity by a large heat capacity can be easily designed [21].

This study reports a detailed cryogenic particle detection measurement scheme with a $CaMoO_4$ crystal as an absorber. A small MMC was used to study the detector performances for both 5.5 MeV alpha and 60 keV gamma absorption. High energy resolutions were achieved for both types of radiation over a wide range of input energies. The thermal properties of $CaMoO_4$ were also investigated at various temperatures to study the feasibility of a $0\nu\beta\beta$ search with a large crystal.

2. Experimental details

A schematic diagram of the experimental setup is shown in Fig. 1. $CaMoO_4$ was wire-cut into a 1 cm × 1 cm × 0.6 cm cuboid from a larger single crystal that had been grown by the Czochralski method with reduced radioactive impurities [11]. The crystal was irradiated with radiation from a thin-layer ^{241}Am source. The major alpha lines of ^{241}Am are 5485.6, 5442.9, and 5388.3 keV with 84.5%, 13.2%, and 1.7% intensity, respectively [24]. A collimator made of a 0.5-mm-thick brass plate was placed between the source and the crystal. In the middle of the plate, a 1-mm diameter hole was made to set the alpha rate to 1 count per second (cps). However, a significant amount of 59.54 keV gammas penetrated

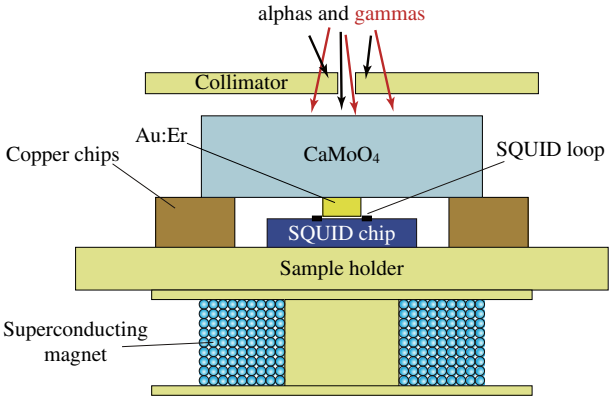

Fig. 1. A schematic diagram of the detector setup (not to scale). Alphas and gammas from an ^{241}Am source are absorbed in a $CaMoO_4$ crystal. The resulting increase in temperature is measured by an MMC with a Au:Er sensor positioned in the pick-up loop of a dc-SQUID. A superconducting magnet is used to magnetize the Au:Er sensor.

through the metal plate and were absorbed by the $CaMoO_4$ crystal. The resulting gamma event rate was about 20 cps.

The absorption of alphas and gammas in the $CaMoO_4$ leads to the emission of scintillation light and changes the temperature of the crystal. In the present experiment, only the temperature response was measured with an MMC. A paramagnetic gold alloy doped with 800 ppm erbium, Au:Er, was used as the MMC sensor material. The increase in temperature induced in the crystal by the absorption of energy was transferred to the attached Au:Er sensor, decreasing its magnetization. The change in magnetization caused a change in the magnetic flux inside the pick-up loop of a dc-SQUID (Superconducting QUantum Interference Device), which converted the flux change to a voltage signal. In this way, the temperature change was accurately measured with a 12-bit digitizer.

A cylindrical Au:Er sensor, laser-machined to have a 40-μm diameter and a 30-μm height, was attached to a thin gold film evaporated on one surface of the crystal. The gold film was 200-nm thick and patterned in a washer shape with a 1-mm outer diameter and a 20-μm inner diameter. The center hole indicated the location of the Au:Er sensor. This gold film was needed to ensure a good thermal and mechanical connection between the $CaMoO_4$ absorber and the Au:Er temperature sensor [25].

The absorber-sensor assembly was then placed over the dc-SQUID in such a way that the Au:Er sensor was aligned with the SQUID pick-up loop. The crystal was supported on each side by four copper chips whose height was meant to minimize the distance between the Au:Er sensor and the SQUID chip without allowing them to touch each other. A small superconducting magnet that can be operated with a persistent current was placed underneath the sample holder to magnetize the paramagnetic Au:Er sensor. Under the experimental conditions used here, the signal size was proportional to the strength of the applied magnetic field. The whole setup containing the absorber-sensor assembly, the SQUID, the magnet, and the ^{241}Am source was enclosed by a 5-mm-thick niobium box and attached to the mixing chamber of a dilution refrigerator.

The signals in this cryogenic particle detector originate from temperature increase due to energy deposit from alphas, gammas, or double beta decay events (i.e. two electrons in this case). Although initial energy loss mechanisms may result in different light yields for different particles in ionizing absorption processes, most of their energy is eventually transferred into the phonon system of the crystal lattice of the detector.

Several heat flow mechanisms are involved in measuring the crystal temperature with the Au:Er sensor. The major portion of

the energy transferred from each particle's absorption spreads out, creating high-energy non-thermal phonons in the $CaMoO_4$ lattice beside the scintillating lights. After successive down-conversion processes, the phonons are thermally distributed in the crystal. For the crystal temperature to be measured with the attached Au:Er sensor, the energy of the phonons should be transmitted to the electrons in the gold film via electron–phonon interactions [25], which cause the major thermal impedance of the heat flow in the experimental conditions. Once the electrons are heated, the heat diffuses relatively quickly in the film and the Au:Er sensor. In turn, the magnetization of the Au:Er sensor changes efficiently along with the temperature change of the electrons due to strong interactions between the spins of erbium ions and the conduction electrons in the Au:Er sensor. The heat gradually flows to a heat bath, the four metal chips through the glue material between the crystal and the metal chips, and thus the temperature of the absorber returns to the initial temperature.

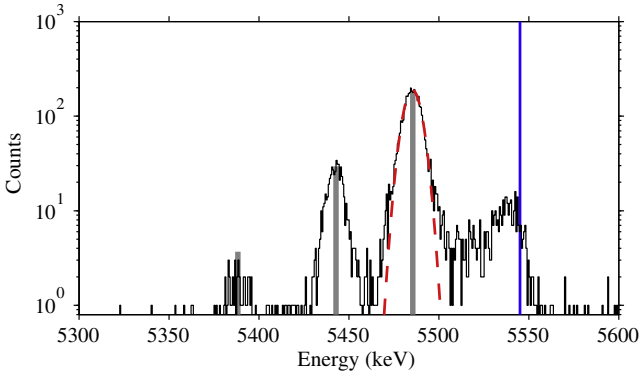

Fig. 3. The ^{241}Am alpha spectrum. The three thick gray lines correspond to three major alpha lines and have appropriate relative intensities. The dashed curve is a Gaussian fit with an 11.2 keV FWHM. The long vertical line indicates the energy 60 keV higher than the most probable alpha line.

3. The energy spectrum

The temperature pulses measured with the detector setup are clearly divided into two groups with a large difference in energy, as shown in Fig. 2. No significant numbers of events were found between the two groups. The alpha particles absorbed in the crystal through the collimator hole result in large pulses and appear around the relative pulse size of unity. The majority of the heat signals appearing in the low energy region are due to the absorption of 59.54 keV gammas. The gamma signals were largely present along with the alpha signals because the detector has a relatively long thermal relaxation time, particularly at low temperatures. The inset of Fig. 2 shows a typical alpha signal together with the gamma pile-ups.

The alpha and gamma spectra were taken individually using different dynamic ranges of the 12-bit digitizer. Fig. 3 shows a ten-hour alpha spectrum that was obtained after applying the cut criteria for pile-up reduction. An optimal filtering method was used to determine the signal size relative to the most frequent alpha pulses [26]. The energy calibration was carried out with the three distinct peaks. The full width at half maximum value (FWHM) of the tallest peak is 11.2 keV. On the right hand side, the tallest peak has a smaller but broader peak at around 60 keV higher energy. This peak is created by the gamma pile-ups with the alpha signals and the alpha-gamma coincidences.

The detector's performance, in particular the measured energy resolution, was degraded by the pile-ups and coincidences with the low-energy gammas, as shown by comparing the energy resolution of the alpha spectrum with that of the baselines. The resolution of the baselines in the absence of any noticeable pulse was measured as 4.1 keV by the optimal filtering method. The difference indicates that the measured resolution of the alpha spectrum was more affected by some features other than the signal-to-noise ratio. The frequent low energy pulses should be one of the main suspects of broadening the spectrum. The statistical fluctuations of lattice damage in the absorber created by the incident alpha particles may have contributed small portion to the difference between the measured and expected resolutions [27]. Moreover, although a thin layer of ^{241}Am was used, the straggling effect from the source may have broadened the energy of the alpha particles. The spectrum provided by the manufacturer of the commercial ^{241}Am source showed 13 keV FWHM with their surface barrier detector, which is worse than the result of the current measurement. An energy resolution close to the one expected from the baseline analysis could have been achieved with a mono-energetic electron source.

The spectrum in Fig. 3 was measured with an applied magnetic field of 1.2 mT. When the magnetic field was increased, the signal size increased in proportion to the strength of the field while the noise level of the SQUID remaining almost the same up to magnetic field of 5 mT. As a result, higher signal-to-noise ratios were obtained by increasing the strength of the field. However, the large signal sizes of typical alpha particles, which are already close to the maximum signal size that the SQUID electronics can generate in a low-noise measurement setup, prevented us from increasing the strength of the magnetic field further to achieve a better signal-to-noise ratio; that is, a better temperature sensitivity. Therefore, using a larger crystal would have allowed for a better performance by increasing the strength of the magnetic field.

Fig. 4 presents a low-energy spectrum obtained with a low trigger level. While the low-energy spectrum taken with the same

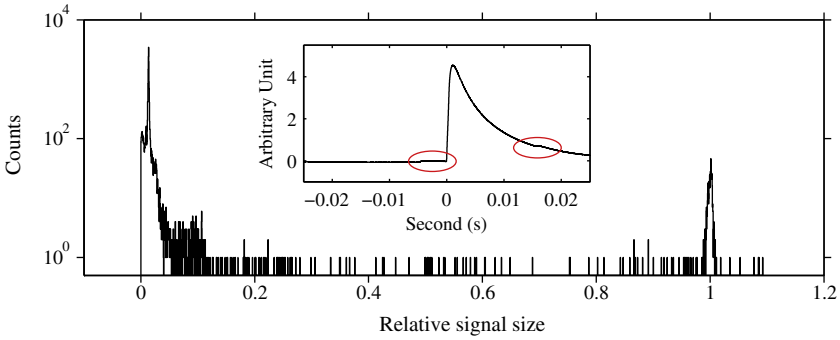

Fig. 2. The distribution of the signal size relative to the most frequent alpha signals on a logarithmic scale. Most low-energy events are in the range of less than 10% of the alpha signal size. The inset shows a single alpha pulse at 35 mK and 1.5 mT with small gamma pulses added as marked with the red circles.

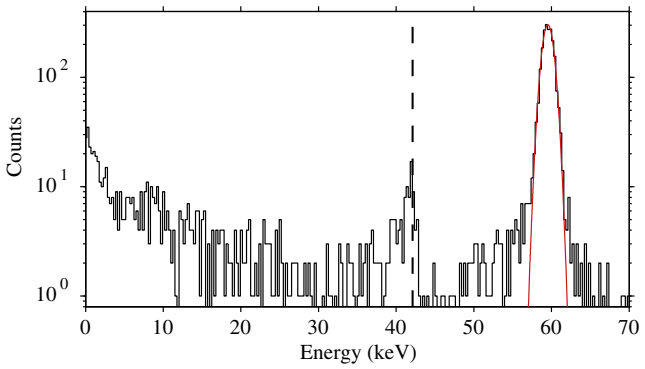

Fig. 4. The low energy spectrum of ^{241}Am. The FWHM of the 59.54 keV peak is 1.7 keV. The red curve is a Gaussian fit to the peak. Another peak around the dashed line originates from the loss of K_α X-ray emissions of molybdenum after the photoelectric absorption of the gamma rays. (For interpretation of the references to color in this figure legend, the reader is referred to the web version of this article.)

conditions as the alpha spectrum except for the trigger level showed an energy resolution comparable to that of the baseline, the applied magnetic field was increased to 2.4 mT for high-resolution gamma spectroscopy. In this condition, all of the alpha signals reset the SQUID electronics and were not recorded. The dominant peak in the figure originated from the full absorption of the 59.54 keV gamma rays because the attenuation length of the gamma ray in the $CaMoO_4$ crystal was about 1 mm. The energy scale was linearly calibrated to set the peak location at the gamma line. The signal size was assumed to be proportional to the absorbed energy in this range because the total heat capacity variation from a 60 keV input at a base temperature of 30 mK is negligible. The FWHM of the dominant peak was 1.7 keV. Another subtle peak was observed to the left of the dominant peak at around 42 keV along the dashed line in Fig. 4. This peak is due to X-ray escape from the crystal caused by molybdenum fluorescence by 59.54 keV in $CaMoO_4$. The K_α emission lines of molybdenum are 17.37 and 17.48 keV [28]. Other peaks from the low-energy radiation of ^{241}Am, such as electrons or low-energy x-rays and gamma rays, do not appear in the spectrum because they are not likely to penetrate the collimator body, and the expected count rates of the radiation through the collimation hole are too low to be distinct.

4. Heat capacity analysis

The fact that the MMC can operate at various temperatures and magnetic fields was used to measure the increase in temperature from the absorption of an alpha particle between 33 mK and 80 mK. The MMC temperatures were calibrated by comparing the DC baseline of the MMC signal with a calibrated RuO_2 thermometer over a wide temperature range. The temperature changes plotted in Fig. 5(a) were converted from the instantaneous heights of each alpha pulse at the onset of the pulse. As shown in the inset of the figure, the pulse heights at their onsets were obtained by the extrapolation of two decay parts of three exponential functions, the best fit to the pulses. The increase in temperature is not small compared to the base temperature. The data points scatter in a vertical distribution because the values for all triggered signals are shown, and the largest bandwidth of the SQUID electronics was used during this measurement for better stability rather than high resolution.

The expected values for instantaneous temperature increase are also shown in Fig. 5(a) for comparison to the measured values. Given an energy input E, the temperate increase ΔT can be found by solving

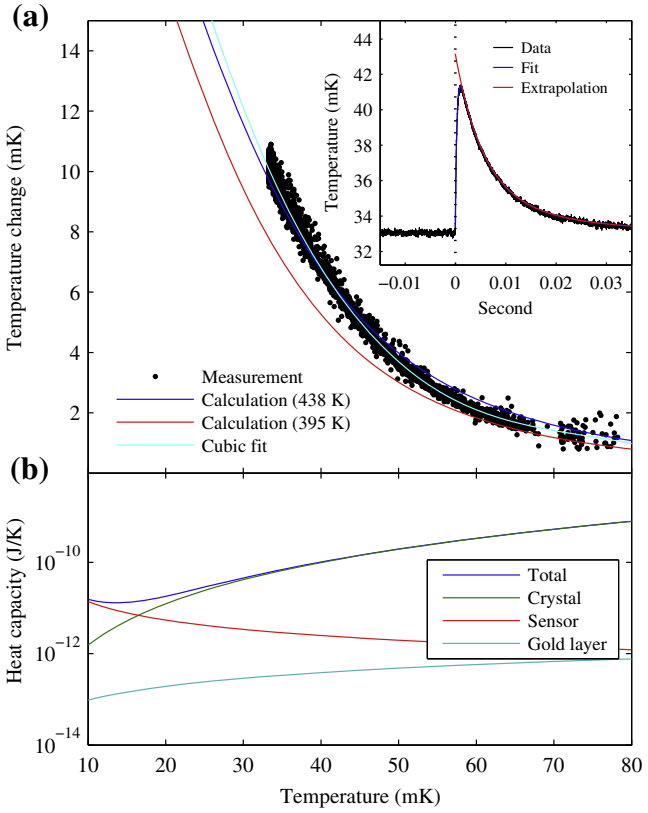

Fig. 5. (a) The temperature changes measured from the absorption of an alpha particle with varying temperatures. The red and blue curves present the temperature changes calculated assuming Debye temperatures of $CaMoO_4$ of 395 K and 438 K, respectively, and the sky-blue curve presents a cubic polynomial function fitted to the measured data. Inset: the alpha heat pulse converted to temperature scale at 33 mK is fit to the sum of the three exponential functions. The temperature change is determined as an extrapolated height of the pulse at the onset. (b) The theoretical total heat capacity and those of the following subsystems: the $CaMoO_4$ crystal, the Au:Er sensor, and the gold film.

$$E = \int_{T_0}^{T_0+\Delta T} C_{tot}(T)dT \tag{1}$$

where T_0 is the base temperature and $C_{tot}(T)$ is the sum of the temperature-dependent heat capacities of the constituent subsystems in the detector, which are the $CaMoO_4$ crystal, the gold film, and the Au:Er sensor. The direct heat flow from non-thermal phonons to the temperature sensor is not considered in the equation. The Debye temperature of $CaMoO_4$ for the heat capacity of the $CaMoO_4$ crystal was found to be 395 K (thermal) or 438 K (elastic), depending on the measurement methods [29]. The red and blue curves in the figure correspond to the calculated temperature increase based on Debye temperatures of 395 K and 438 K, respectively. The measured data agree better with the calculation using the elastic Debye temperature than the calculation using the thermal one. In both cases, however, the measured values are larger than the values expected based on the thermal equilibrium model at lower temperatures, even though the initial energy loss to the creation of scintillation lights is not considered. The direct energy transfer from the non-thermal phonons to the electrons in the gold film may be responsible for the increased signal size because the non-thermal phonon process is more efficient at lower temperatures where the thermal heat flow processes become slow.

The theoretical heat capacities of the subsystems are plotted in Fig. 5(b). This calculation used an elastic Debye temperature of 438 K and an applied magnetic field of 0.9 mT, the same conditions

as the measurement of the increase in temperature. The major contribution of C_{tot} is from the absorber crystal in the temperature range considered in the experiment.

5. Discussion

Two of the main strategies of improving the sensitivity in $0\nu\beta\beta$-search experiments are to house more massive detectors and to improve the energy resolution. However, these two strategies are in competition in the general case of thermal detectors. One approach to solving this problem is to use many crystals for individual measurement cells instead of one large crystal. In order to design a cost-effective experiment, it is important to find an optimal crystal size with enough sensitivity for the application. For instance, each measurement cell can contain a $CaMoO_4$ crystal with $4 \sim 5$ cm diameter and $4 \sim 5$ cm height in cylindrical shape.

The heat capacity analysis indicates that the increase in temperature of a $CaMoO_4$ crystal due to an energy input can be obtained from the heat flow model with known thermal property values. As discussed above, the energy resolution in the absence of pile-ups is expected to be better than the measured one, and to be better still if several times larger crystals were used with the current Au:Er sensor because there is room to increase the detector's sensitivity. A similar argument can be made for the size of the Au:Er sensor. As the heat capacity of the $CaMoO_4$ crystal is much larger than that of the magnetic sensor, using a sensor with a larger number of spins would not affect the instantaneous temperature increase, but it would provide a larger signal size. Furthermore, because the energy resolution of thermal detectors with an MMC optimally designed for a given absorber heat capacity C_a is proportional to $(C_aT)^{-1/2}$ [21], more flexibility in crystal volume is allowed at lower temperatures. Considering that the energy resolution of MMCs achieved in X-ray spectroscopy is better than 1/2000, it seems achievable to find a resolution on the order of $1 \sim 2$ keV for a 3 MeV energy input with a realistic size of 250 g $CaMoO_4$ crystal, about 100 times larger than the current crystal.

An additional light detector can be introduced to improve the energy resolution as well as the radioactive background rejection by measuring scintillation light simultaneously. Silicon and germanium wafers seem to be appropriate as light absorbers, and the signal could be measured with an additional cryogenic detector. In addition, we will also investigate the shape difference between the phonon signals from alpha and gamma in a few MeV region as suggested by [30].

$CaMoO_4$ crystals about 250 g of mass with reduced radioactive impurities have been successfully grown using molybdenum enriched on ^{100}Mo and calcium depleted on ^{48}Ca [31]. Internal backgrounds of the crystals are under test at the Yangyang Underground Laboratory. As a final goal, we are going to develop a large scale high sensitivity experiment to search for $0\nu\beta\beta$ decay of ^{100}Mo by using enriched ^{100}Mo in calcium molybdate crystals as cryogenic scintillating bolometers.

Acknowledgements

The work at KRISS was supported by Internal Creative Research Funds at KRISS and the NRF Radiation Technology Development Program funded by MEST. The work at Seoul National University was supported by World Class University Project of National Research Foundation of Korea. S.J. Lee acknowledges support from Seoul Fellowship. V.V. Kobychev acknowledges support from the Brain Pool Program. The group from the Institute for Nuclear Research (Kyiv, Ukraine) was supported in part through the grant M/361-2008 of the State Fund for Fundamental Researches of Ukraine. The group from ITEP was supported in part through the grant ISTC 3893 and grant of the Federal Science and innovations Agency of Russian Federation (Federal Aiming Program project 2008-03-1.3-25-09-015).

References

[1] W.H. Furry, On transition probabilities in double beta-disintegration, Physical Review 56 (12) (1939) 1184–1193, doi:10.1103/PhysRev.56.1184.
[2] V.I. Tretyak, Y.G. Zdesenko, Tables of double beta decay data – an update, Atomic Data and Nuclear Data Tables 80 (1) (2002) 83–116, doi:10.1006/adnd.2001.0873.
[3] Y. Fukuda, T. Hayakawa, E. Ichihara, K. Inoue, K. Ishihara, H. Ishino, Y. Itow, T. Kajita, J. Kameda, S. Kasuga, et al., Evidence for oscillation of atmospheric neutrinos, Physical Review Letters 81 (8) (1998) 1562–1567.
[4] E. Majorana, Theory of the symmetry of electrons and positrons, Nuovo Cimento 14 (1937) 171–184.
[5] H.V. Klapdor-Kleingrothaus, A. Dietz, H.L. Harney, I.V. Krivosheina, Evidence for neutrinoless double beta decay, Modern Physics Letters A 16 (37) (2001) 2409–2420.
[6] R. Arnold, C. Augier, J. Baker, A. Barabash, G. Broudin, V. Brudanin, A. Caffrey, E. Caurier, V. Egorov, K. Errahmane, et al., First results of the search for neutrinoless double-beta decay with the NEMO 3 detector, Physical Review Letters 95 (18) (2005) 182302.
[7] S. Schönert, I. Abt, M. Altmann, A.M. Bakalyarov, I. Barabanov, C. Bauer, M. Bauer, E. Bellotti, S. Belogurov, S.T. Belyaev, A. Bettini, L. Bezrukov, V. Brudanin, C. Büttner, V.P. Bolotsky, A. Caldwell, C. Cattadori, M.V. Chirchenko, O. Chkvorets, H. Clement, E. Demidova, A.D. Vacri, J. Eberth, V. Egorov, E. Farnea, A. Gangapshev, G.Y. Grigoriev, V. Gurentsov, K. Gusev, W. Hampel, G. Heusser, W. Hofmann, L.V. Inzhechik, J. Jochum, M. Junker, S. Katulina, J. Kiko, I.V. Kirpichnikov, A. Klimenko, K.T. Knöpfle, O. Kochetov, V.N. Kornoukhov, R. Kotthaus, V. Kusminov, M. Laubenstein, V.I. Lebedev, X. Liu, H.-G. Moser, I. Nemchenok, L. Pandola, P. Peiffer, R.H. Richter, K. Rottler, C.R. Alvarez, V. Sandukovsky, S. Schönert, S. Scholl, J. Schreiner, B. Schwingenheuer, H. Simgen, A. Smolnikov, A.V. Tikhomirov, C. Tomei, C.A. Ur, A.A. Vasenko, S. Vasiliev, D. Weißhaar, M. Wojcik, E. Yanovich, J. Yurkowski, S.V. Zhukov, G. Zuzel, The GERmanium Detector Array (Gerda) for the search of neutrinoless $\beta\beta$ decays of ^{76}Ge at LNGS, Nuclear Physics B – Proceedings Supplements 145 (2005) 242–245, doi:10.1016/j.nuclphysbps.2005.04.014.
[8] C. Arnaboldi, D. Artusa, F. Avignone III, M. Balata, I. Bandac, M. Barucci, J. Beeman, F. Bellini, C. Brofferio, C. Bucci, et al., Results from a search for the $0\nu\beta\beta$-decay of ^{130}Te, Physical Review C 78 (3) (2008) 035502.
[9] H.J. Kim, et al., A search for the 0-neutrino double beta decay with the $CaMoO_4$ scintillator, in: Proceedings of New Views in Particle Physics (VIETNAM 2004), 2004, pp. 449–454.
[10] S. Belogurov, V. Kornoukhov, A. Annenkov, A. Borisevich, A. Fedorov, M. Korzhik, V. Ligoun, O. Missevitch, S. Kim, S. Kim, et al., $CaMoO_4$ Scintillation Crystal for the Search of ^{100}Mo Double Beta Decay, IEEE Transactions on Nuclear Science 52 (4) (2005) 1131–1135.
[11] A.N. Annenkov, O.A. Buzanov, F.A. Danevich, A.S. Georgadze, S.K. Kim, H.J. Kim, Y.D. Kim, V.V. Kobychev, V.N. Kornoukhov, M. Korzhik, et al., Development of $CaMoO_4$ crystal scintillators for a double beta decay experiment with ^{100}Mo, Nuclear Instruments and Methods in Physics Research A 584 (2008) 334–345.
[12] S. Rahaman, V. Elomaa, T. Eronen, J. Hakala, A. Jokinen, J. Julin, A. Kankainen, A. Saastamoinen, J. Suhonen, C. Weber, et al., Q values of the ^{76}Ge and ^{100}Mo double-beta decays, Physics Letters B 662 (2) (2008) 111–116.
[13] M.E. Wieser, J.R.D. Laeter, Absolute isotopic composition of molybdenum and the solar abundances of the p-process nuclides ^{92,94}Mo, Physical Review C 75 (5) (2007) 055802, doi:10.1103/PhysRevC.75.055802.
[14] S. Pirro, J. Beeman, S. Capelli, M. Pavan, E. Previtali, P. Gorla, Scintillating double-beta-decay bolometers, Physics of Atomic Nuclei 69 (12) (2006) 2109–2116.
[15] P. Gorla, C. Arnaboldi, J. Beeman, S. Capelli, A. Giachero, L. Gironi, M. Pavan, G. Pessina, S. Pirro, E. Previtali, Scintillating bolometers for double beta decay search, Journal of Low Temperature Physics 151 (3) (2008) 854–859.
[16] O. Barinova, F. Danevich, V. Degoda, S. Kirsanova, V. Kudovbenko, S. Pirro, V. Tretyak, First test of Li_2MoO_4 crystal as a cryogenic scintillating bolometer, Nuclear Instruments and Methods in Physics Research Section A: Accelerators, Spectrometers, Detectors and Associated Equipment 613 (1) (2010) 54–57, doi:10.1016/j.nima.2009.11.059.
[17] L. Gironi, C. Arnaboldi, J.W. Beeman, O. Cremonesi, F.A. Danevich, V. Degoda, L.I. Ivleva, L.L. Nagornaya, M. Pavan, G. Pessina, S. Pirro, V.I. Tretyak, I.A. Tupitsyna, Performance of $ZnMoO_4$ crystal as cryogenic scintillating bolometer to search for double beta decay of molybdenum, Journal of Instrumentation 5 (11) (2010) P11007, doi:10.1088/1748-0221/5/11/P11007.
[18] L. Nagornaya, F. Danevich, A. Dubovik, B. Grinyov, S. Henry, V. Kapustyanyk, H. Kraus, D. Poda, V. Kudovbenko, V. Mikhailik, M. Panasyuk, O. Polischuk, V. Rudyk, V. Tsybulskyi, I. Tupitsyna, Y. Vostretsov, Tungstate and molybdate scintillators to search for dark matter and double beta decay, IEEE Transactions on Nuclear Science 56 (4) (2009) 2513–2518, doi:10.1109/TNS.2009.2022268.
[19] J.I. Lee, W.G. Kang, Y.D. Kim, A test on a $CaMoO_4$ crystal coupled with a LAAPD for a double beta-decay experiment, Journal of the Korean Physical Society 56 (3) (2010) 733–736.
[20] Y.G. Zdesenko, F.A. Danevich, V.I. Tretyak, Sensitivity and discovery potential of the future 2β decay experiments, Journal of Physics G: Nuclear and Particle

Physics 30 (9) (2004) 971–981. Available from: http://stacks.iop.org/0954-3899/30/i=9/a=002.
[21] A. Fleischmann, C. Enss, G.M. Seidel, Metallic magnetic calorimeters, Topics in Applied Physics 99 (2005) 151–216.
[22] S.J. Lee, M.K. Lee, Y.S. Jang, I.H. Kim, S.K. Kim, J.S. Lee, K.B. Lee, Y.H. Lee, Y.H. Kim, Cryogenic measurement of alpha decay in a 4π absorber, Journal of Physics G: Nuclear and Particle Physics 37 (2010) 055103.
[23] M. Loidl, M. Rodrigues, B. Censier, S. Kowalski, X. Mougeot, P. Cassette, T. Branger, D. Lacour, Metallic Magnetic Calorimeters for Beta Spectrometry, in: AIP Conference Proceedings, vol. 1185, 2009, pp. 587–590.
[24] M.-M. Bé, V. Chisté, C. Dulieu, E. Browne, C. Baglin, V. Chechev, N. Kuzmenko, R. Helmer, A. Nichols, E. Schönfeld, R. Dersch, Table of radionuclides, 2004, BIPM Monographie 5.
[25] Y.H. Kim, H. Eguchi, C. Enss, Y.H. Huang, R.E. Lanou, H.J. Maris, A.N. Mocharnuk-Macchia, G.M. Seidel, B. Sethumadhavan, W. Yao, Measurements and modeling of the thermal properties of a calorimeter having a sapphire absorber, Nuclear Instruments and Mechanisms A 520 (2004) 208–211, doi:10.1016/j.nima.2003.11.230.
[26] A.E. Szymkowiak, R.L. Kelley, S.H. Moseley, C.K. Stahle, Signal processing for microcalorimeters, Journal of Low Temperature Physics 93 (3-4) (1993) 281–285, doi:10.1007/BF00693433.
[27] R.D. Horansky, G.M. Stiehl, J.A. Beall, K.D. Irwin, A.A. Plionis, M.W. Rabin, J.N. Ullom, Measurement of ion cascade energies through resolution degradation of alpha particle microcalorimeters, Journal of Applied Physics 107 (2010) 044512.
[28] A. Thompson, D. Attwood, E. Gullikson, M. Howells, K.J. Kim, J. Kirz, J. Kortright, I. Lindau, P. Pianatta, A. Robinson, et al., X-ray Data Booklet, Lawrence Berkeley National Laboratory, 2001. pp. 1–38.
[29] A. Senyshyn, H. Kraus, V.B. Mikhailik, L. Vasylechko, M. Knapp, Thermal properties of $CaMoO_4$: lattice dynamics and synchrotron powder diffraction studies, Physical Review B 73 (1) (2006) 014104.
[30] L. Gironi, Scintillating bolometers for double beta decay search, Nuclear Instruments and Methods in Physics Research Section A: Accelerators, Spectrometers, Detectors and Associated Equipment 617 (1–3) (2010) 478–481. Proceedings of the 11th Pisa Meeting on Advanced Detectors, doi:10.1016/j.nima.2009.10.080.
[31] V. Kornoukhov, First results of $^{40}Ca^{100}MoO_4$ single crystals growing for Astroparticle Physics application, in: International Workshop on Double Beta Decay Search, 15–17 October 2009, Seoul National University, Seoul, Korea, <http://q2c.snu.ac.kr/indico/conferenceDisplay.py?confid=11>.